JOURNAL OF APPLIED ELECTROCHEMISTRY 16 (1986) 591–604

Kinetics of copper electrodeposition in citrate electrolytes

E. CHASSAING*, K. VU QUANG

Centre d'Etudes de Chimie Métallurgique du CNRS, 15 rue Georges Urbain, 9440 Vitry, France

R. WIART

Laboratoire propre no 15 du CNRS, 'Physique des Liquides et Electrochimie', associé à l'Université Pierre et Marie Curie, 4 Place Jussieu, 75230 Paris Cedex 05, France

Reveived 10 July 1985; revised 10 September 1985

The kinetics of copper electrocrystallization in citrate electrolytes (0.5 M $CuSO_4$, 0.01 to 2 M sodium citrate) and citrate ammonia electrolytes (up to pH 10.5) were investigated. The addition of citrate strongly inhibits the copper reduction. For citrate concentrations ranging from 0.6 to 0.8 M, the impedance plots exhibit two separate capacitive features. The low frequency loop has a characteristic frequency which depends mainly on the electrode rotation speed. Its size increases with increasing current density or citrate concentration and decreases with increasing electrode rotation speed. A reaction path is proposed to account for the main features of the reduction kinetics (polarization curves, current dependence of the current efficiency and impedance plots) observed in the range 0.5 to 0.8 M citrate concentrations. This involves the reduction of cupric complex species into a compound that can be either included as a whole into the deposit or decomplexed to produce the metal deposit. The resulting excess free complexing ions at the interface would adsorb and inhibit the reduction of complexed species. With a charge transfer reaction occurring in two steps coupled by the soluble Cu(I) intermediate which is able to diffuse into the solution, this model can also account for the low current efficiencies observed in citrate ammonia electrolytes and their dependencies upon the current density and electrode rotation speed.

Nomenclature

b, b_1, b_1^*	Tafel coefficients (V^{-1})
$\mathscr{C}$	bulk concentration of complexed species ($mol\,cm^{-3}$)
$\mathscr{C}^*$	concentration of intermediate C* at $x = 0$ ($mol\,cm^{-3}$)
C	concentration of $(Cu\ Cit\ H)^{2-}$ at $x = 0$ ($mol\,cm^{-3}$)
ΔC	C variation due to ΔE
C'	concentration of complexing agent $(Cit)^{3-}$ at the distance x ($mol\,cm^{-3}$)
C'_0	concentration C' at $x = 0$ ($mol\,cm^{-3}$)
$\Delta C'_0$	C'_0 variation due to ΔE
C'_s	bulk concentration C' ($mol\,cm^{-3}$)
(Cit H), (Cu), (Compl)	molecular weights (g)
C_{dl}	double layer capacitance ($F\,cm^{-2}$)
D	diffusion coefficient of $(Cit)^{3-}$ ($cm^2\,s^{-1}$)
D_1	diffusion coefficient of C* ($cm^2\,s^{-1}$)
E	electrode potential (V)
f_1	frequency in Equation 25 (s^{-1})

* To whom all correspondence should be addressed.

0021–891X/86 $03.00 + .12

F	Faraday's constant (96 500 A s mol^{-1})
i, i_1, i_1^*	current densities (A cm^{-2})
Δi	i variation due to ΔE
$Im(Z)$	imaginary part of Z
j	$\sqrt{-1}$
k_1, k_1^*, K_1, K_1^*, K_2, K'	rate constants (cm s^{-1})
K	rate constant (s^{-1})
K_3	rate constant (cm^3 A^{-1} s^{-1})
R_t	transfer resistance (Ω cm^2)
R_p	polarization resistance (Ω cm^2)
$Re(Z)$	real part of Z
t	time (s)
x	distance from the electrode (cm)
Z_f	faradaic impedance (Ω cm^2)
Z	electrode impedance (Ω cm^2)

Greek symbols

β	maximal surface concentration of complexing species (mol cm^{-2})
δ	thickness of Nernst diffusion layer (cm)
η, η_1, η_2	current efficiencies
ω	angular frequency (rad s^{-1})
Ω	electrode rotation speed (rev min^{-1})
τ	$= K^{-1}$ (s)
τ_d	diffusion time constant (s)
θ	electrode coverage by adsorbed complexing species
θ_0	electrode coverage due to C_s'
$\Delta\theta$	θ variation due to ΔE

1. Introduction

In previous work the electrolysis conditions for the electrodeposition of Ni–Cu alloy layers were determined [1]. Due to the largely different reduction potentials of Ni^{2+} and Cu^{2+} ions, complexing agents are necessary to achieve the codeposition of the two metals; citrate or pyrophosphate anions were found to be the most efficient ones [2, 3]. Few investigations have been devoted to the electrocrystallization of metals and alloys in complexing solutions. With the aim of investigating the codeposition kinetics of nickel and copper the electroreduction of cupric ions in the presence of citrate had to be understood. Though the reduction of cupric ions in the sulphate–acid solutions has been thoroughly investigated ([4] and references therein), the effect of complexing agents such as citrate and/or ammonia has been studied only in low concentration solutions (10^{-3} M $CuSO_4$) [5, 6]. It is often assumed that complexed ions are reduced without prior dissociation [7]. However only steady-state experiments have been performed and no detailed mechanism has been so far developed. The present work was aimed at a better understanding of the reduction kinetics of complexed cupric species with the aid of electrode impedance measurements.

2. Experimental procedure

The electrolytes were made up of analytical grade purity chemicals Prolabo R.P. (min 99%) dissolved in double distilled water. The copper sulphate concentration was 0.5 M and the trisodium citrate concentration ($Na_3C_6H_5O_7 \cdot 2H_2O$) was varied between 0.01 and 2 M. The temperature was held at 25° C and the solutions were deoxygenated by high purity 'U'-nitrogen bubbling.

The counterelectrode was a large area oxygen free high conductivity copper plate. The working electrode was a copper disc of 0.20 or 0.28 cm^2 area rotating at a speed of up to 2000 rev min^{-1}. Before each experiment the working electrode was polished with emery paper (1200 grade).

The steady-state current–potential curves were galvanostatically recorded. All potentials were referred to the saturated mercurous sulphate electrode (SSE) and corrected for ohmic drop. The electrode impedance was measured using a frequency response analyser between 10 kHz and 10^{-3} Hz.

3. Results

3.1. *Current–potential curves*

For pure 0.5 M $CuSO_4$ electrolyte (Fig. 1, Curve 1) the polarization curve does not depend on the rotation speed of the electrode between 320 and 2000 rev min^{-1}, up to 70 mA cm^{-2}. Increasing citrate additions to copper sulphate electrolytes (Curves 2 to 9) shift the polarization curve for copper reduction towards increasingly negative potentials. In the range of 0.01 to 0.1 M citrate concentrations (Curves 2 and 3) and at low cathode polarizations, both the current density and the current efficiency decrease as the rotation speed increases, thus indicating the solubility of the Cu(I) intermediate stabilized by complexing ions. For larger citrate additions an opposite trend is observed: for a given potential the current increases with the rotation speed and this effect becomes more pronounced with increasing citrate concentration.

Depending on pH and on citrate/copper ratio different complexes may exist [8, 9]. However the analytical investigations reported so far, have been carried out in more dilute solutions than in the present work. Besides compounds formed with the citrate anions (related to the acid functions of citric acid), polynuclear species may be found; in particular the dinuclear species $Cu_2(Cit)_2^{2-}$ are fairly stable [8, 10]. With increasing citrate concentrations, the electrolyte pH increases progressively from 2.6 for pure 0.5 M $CuSO_4$ to 5.6 for 2 M citrate addition; this pH rise would correspond to the progressive neutralization of hydrogenated citrate ions. The stability of the solutions also depends on the composition; for high copper sulphate/citrate ratios, a precipitate appears within a few hours or a few days. This is likely to be $Cu_2C_6H_4O_7$ as already observed [9]. For citrate concentrations over 0.5 M, the solutions are fairly stable.

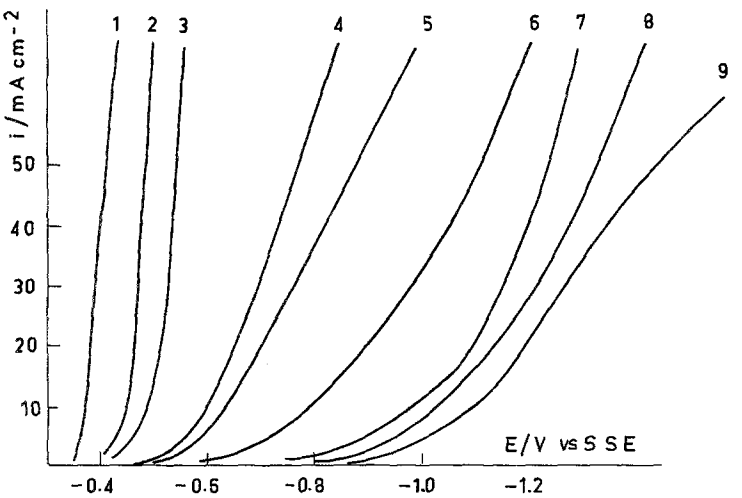

Fig. 1. Steady-state polarization curves for 0.5 M $CuSO_4$ with increasing sodium citrate additions (M): (1) 0; (2) 0.01; (3) 0.10; (4) 0.50; (5) 0.60; (6) 0.75; (7) 1.00; (8) 1.50; (9) 2.00. Rotation speed: 1800 rev min^{-1}.

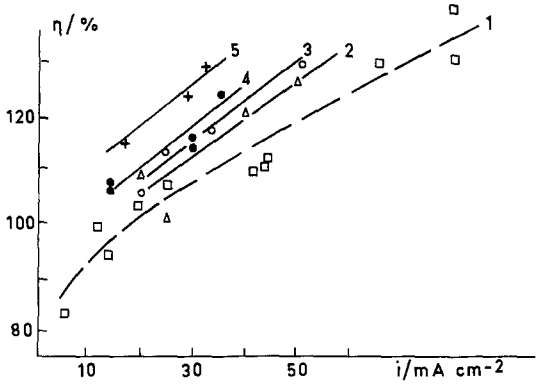

Fig. 2. Current efficiency versus current density curves for 0.5 M $CuSO_4$ with increasing sodium citrate additions (M): (1) (□) 0.50; (2) (△) 0.60; (3) (○) 0.80; (4) (●) 1.00; (5) (+) 1.50. Rotation speed: 900 rev min^{-1}.

3.2. *Current efficiency*

For citrate additions higher than 0.5 M the current efficiency is found to be higher than 100% (Fig. 2). It increases with citrate concentration and almost linearly with current density. For example the efficiency reaches 130% for a deposit performed at 50 mA cm^{-2} from a bath containing 0.8 M sodium citrate.

By thermogravimetric analysis it was verified that organic inclusions were present in the deposits. When heating a deposit, separated from its substrate, a weight loss between 160 and 180° C is recorded. This weight loss, zero for deposits obtained from citrate-free sulphate solution, increases with the current density and the citrate concentration in the bath: for example it varies from 4 to 6% when the current density of deposition from electrolytes containing 0.6 M sodium citrate increases from 20 to 100 mA cm^{-2}.

The inclusion process probably involves complicated reactions with the likely breakdown and chemical transformation of the complexing agent before inclusion, similar to the situation already encountered for the included additives in metal deposition [11–13]. For simplicity it is assumed that the reduced cupric citrate complex is included as a whole. Furthermore if the complex decomposes like citric acid into copper carbonate or oxide with the evolution of organic products, the weight loss recorded in the above mentioned example would yield inclusions increasing from 14 to 20% with current density. This is the order of magnitude of the excess current efficiency.

3.3. *Impedance measurements*

The impedance diagrams recorded either over the whole polarization range with solutions containing more than 0.5 M citrate or at high polarizations with solutions containing 0.01 to 0.1 M citrate exhibit two capacitive features (Fig. 3). The high frequency loop reveals a frequency distribution which is more pronounced with increasing citrate concentration and/or current density. The mean capacity calculated from the apex of the high frequency capacitive loop is around 50 μF cm^{-2} for 0.5 M citrate electrolyte and 80 μF cm^{-2} for 0.6 M. For larger citrate concentrations this capacity increases markedly. This suggests that a relaxation process interferes with the high frequency feature. Above 0.8 M citrate it becomes impossible to estimate the transfer resistance R_t and the double-layer capacity. The $R_t i$ product of the transfer resistance and the current density first increases with current density and then tends towards an approximately constant value of 100 mV (Fig. 4). The size of the low frequency capacitive feature, described by the R_p/R_t ratio, where R_p is the polarization resistance, increases with citrate concentration and almost linearly with current density (Fig. 5). With increasing electrode rotation speed, the size of the loop decreases (Fig. 6). The frequency at the apex, which is nearly independent of the current density or the citrate concentration, is

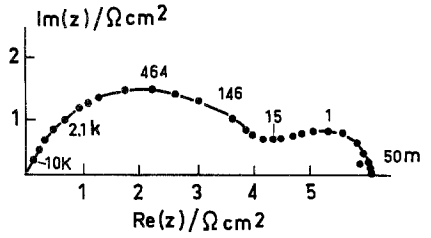

Fig. 3. Complex plane impedance plot recorded in 0.5 M $CuSO_4$, 0.6 M Na_3Cit at 20 mA cm^{-2}, rotation speed 1800 rev min^{-1}.

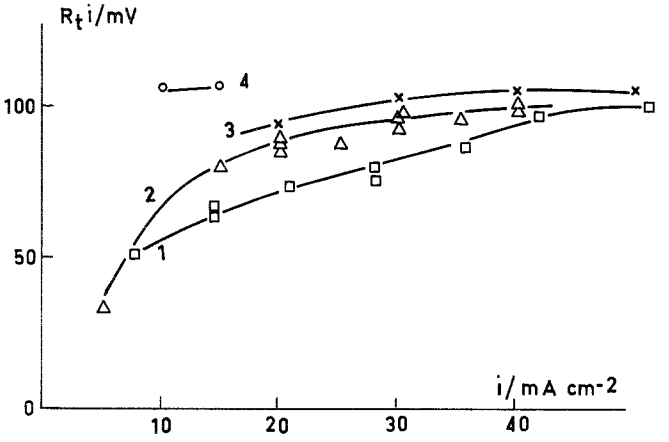

Fig. 4. Current dependence of the $R_t i$ product (transfer resistance × current density) for 0.5 M $CuSO_4$ with sodium citrate additions (M): (1) (□) 0.50; (2) (△) 0.60; (3) (×) 0.70; (4) (○) 0.80. Rotation speed: 1800 rev min^{-1}.

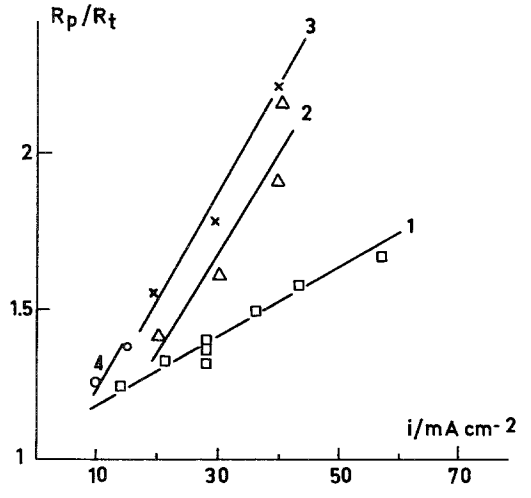

Fig. 5. Current dependence of the R_p/R_t ratio (R_p polarization resistance, R_t transfer resistance) for 0.5 M $CuSO_4$ with sodium citrate additions (M): (1) (□) 0.50; (2) (△) 0.60; (3) (×) 0.70; (4) (○) 0.80. Rotation speed; 1800 rev min^{-1}.

approximately proportional to the rotation speed of the electrode, though there is considerable scatter of the data (Fig. 7).

3.4. *Influence of ammonia additions*

The effect of ammonia additions on Cu(II) reduction in citrate electrolytes depends mainly on the composition of the solution. With increasing ammonia concentration the pH increase suggests the

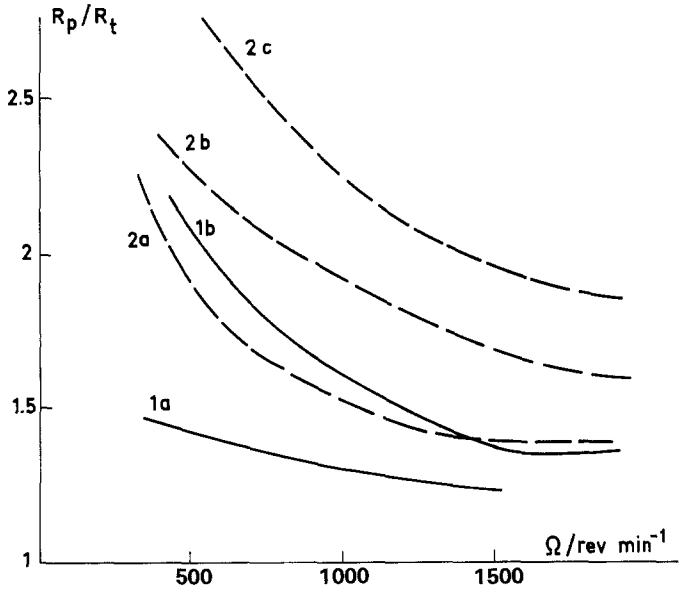

Fig. 6. Rotation speed dependence of the ratio R_p/R_t for 0.5 M $CuSO_4$ with sodium citrate additions (M): (1) 0.50 (a) current density 14.3 mA cm^{-2} (b) current density 28.6 mA cm^{-2}. (2) 0.60 (a) current density 20.0 mA cm^{-2} (b) current density 30.0 mA cm^{-2} (c) current density 40 mA cm^{-2}.

neutralization of the fourth citrate acidity with the likely formation of a mixed citrate ammonia complex [14]. Increasing ammonia additions shift the copper reduction towards more negative values for pHs lower than 8 (Fig. 8, Curve 2). For higher pH values an opposite trend is observed (Fig. 8, Curves 3 to 5). For pHs above 9 the current efficiency is lower than unity and increases with increasing current density and with decreasing electrode rotation speed in agreement with the solubility of the Cu(I) intermediate which diffuses away (Fig. 9, Curves 2a and b). It is noted that even when the efficiency is lower than unity the inclusion of organic products in the deposits occurs as shown by thermogravimetric analysis.

The impedance diagrams recorded at pHs above 9.5, exhibit two capacitive features as in ammonia-free electrolytes. The $R_t i$ product is current independent and slightly decreased as compared to ammonia-free electrolytes (Fig. 10, Curve 1). For a given rotation speed the low frequency capacitive loop has a characteristic frequency close to 1 Hz throughout the polarization range. With citrate electrolytes, with increase of current density, the loop size measured by the R_p/R_t ratio is first nearly constant and then increases (Fig. 10, Curve 2).

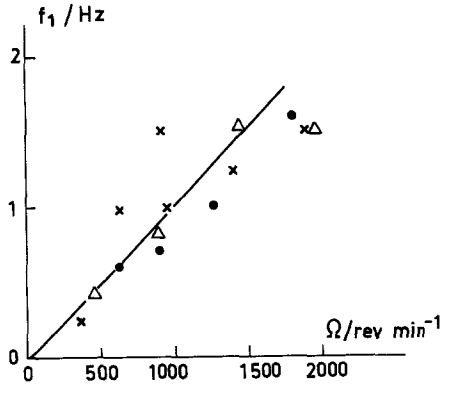

Fig. 7. Characteristic frequency of the low frequency capacitive feature as a function of the electrode rotation speed in 0.5 M $CuSO_4$, 0.6 M Na_3Cit electrolyte. (×) Current density 20 mA cm^{-2} (△) current density 30 mA cm^{-2} (○) current density 40 mA cm^{-2}.

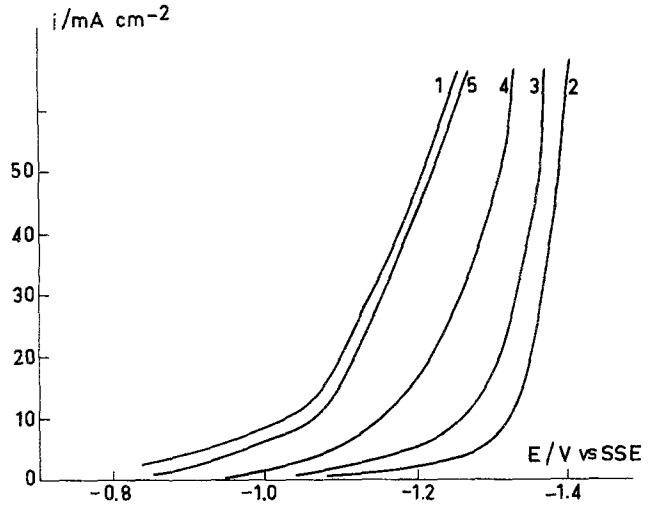

Fig. 8. Steady-state polarization curves for 0.5 M $CuSO_4$ and 1.0 M Na_3Cit with increasing ammonia additions (1) no ammonia pH = 4.8, (2) ammonia to pH = 7.4, (3) ammonia to pH = 8.2, (4) ammonia to pH = 9.3, (5) ammonia to pH = 10.4. Rotation speed: 1800 rev min^{-1}.

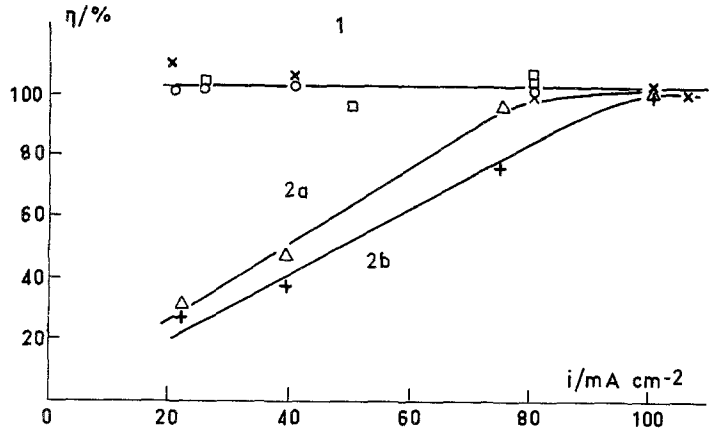

Fig. 9. Current dependence of the current efficiency for 0.5 M $CuSO_4$, 1.0 M Na_3Cit and ammonia. (1) (×) pH = 5.4; (□) pH = 8.2; (○) pH = 9.3, rotation speed: 900 rev min^{-1}. (2a) (△) pH = 10.2, rotation speed 450 rev min^{-1}. (2b) (+) pH = 10.2, rotation speed 900 rev min^{-1}.

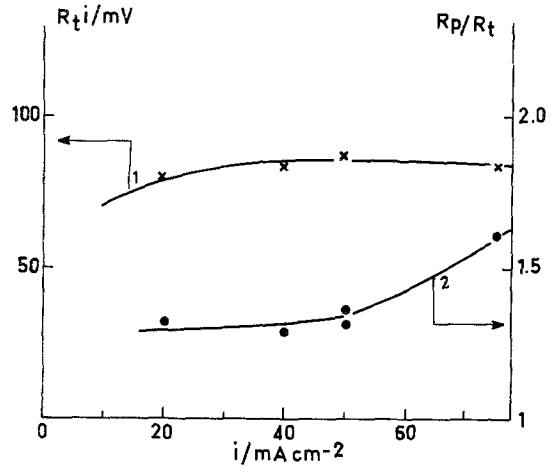

Fig. 10. Current dependence of the $R_t i$ product (Curve 1) and the R_p/R_t ratio (Curve 2) for 0.5 M $CuSO_4$, 1.0 M Na_3Cit and ammonia (pH 10.4). Rotation speed 1800 rev min^{-1}.

4. Discussion

In concentrated solutions it is difficult to be precise about which species are present. For the highest citrate concentrations the dinuclear compound $[Cu_2Cit_2]^{2-}$ would predominate [8]. In the 0.5 to 0.8 M Na_3 citrate concentration range, according to the equilibrium constants of the various copper citrate complexes [15], hydrogenated citrate compounds (written Cu Cit H in the present paper) would predominate.

The following reaction path will be considered:

$$\text{(I)}\quad \text{Cu Cit H} + 2e \xrightarrow{K_1} [\text{Cu Cit H}]^{2-}$$

$$\text{(II)}\quad [\text{Cu Cit H}]^{2-} \xrightarrow{K_2} \text{Cu} + \text{H}^+ + [\text{Cit}]^{3-} \xrightarrow{D} [\text{Cit}]^{3-}_{\text{sol}} \quad \text{(IV)}$$

$$\text{(III)}\quad [\text{Cu Cit H}]^{2-} \xrightarrow{K_3} \text{Included species}$$

$$[\text{Cit}]^{3-} \underset{K}{\overset{K'}{\rightleftharpoons}} [\text{Cit}]^{3-}_{\text{ads}} \quad \text{(V)}$$

The complexed copper compound is reduced without prior decomplexation (Reaction 1), since no limiting current is observed on the polarization curves (Fig. 1). The resulting reduced copper complex $[Cu\ Cit\ H]^{2-}$ either undergoes decomplexation (Reaction II) or is included into the copper deposits (Reaction III). As a consequence of Reaction II, a surface excess of the free complexing agent, denoted $(Cit)^{3-}$, occurs. This anion thus diffuses and probably migrates towards the solution in which it is transformed into complexed copper species (Reaction IV). On the electrode surface the anion also adsorbs thus blocking a traction θ of the electrode area (Reaction V).

The charge transfer (Reaction I) takes place on the unblocked electrode area, $(1 - \theta)$, resulting in a current density i:

$$i = 2FK_1\mathscr{C}(1 - \theta) \tag{1}$$

where $\mathscr{C}$ is the concentration of the complexed cupric species and $K_1 = k_1 \exp(bE)$ as Reaction I is assumed to follow a Tafel activation with potential.

Due to the inclusion of the complexed copper compounds (III) the current efficiency η is higher than unity. The incorporation rate is expressed by K_3Ci since it is generally admitted that the inclusion rate is proportional to the current density and to the surface concentration C of $(Cu\ Cit\ H)^{2-}$ to be included [16]. Ignoring the real compositon of included species, it will be assumed for simplicity that the reduced copper complex produced by Reaction I is entirely included into the deposit thus allowing η to be expressed by:

$$\eta = 1 + \frac{K_3 i \dfrac{(Cit\ H)}{(Cu)}}{K_2 + K_3 i} \tag{2}$$

where $(Cit\ H)$ and (Cu) are the respective molecular weights.

4.1. *Material balances*

4.1.1. Reduced copper complex, C. The rate constant K_2 is assumed to be so high that the concentration C of $(Cu\ Cit\ H)^{2-}$ follows a change in current density very rapidly (pseudo-equilibrium). Thus it is given by:

$$\frac{i}{2F} - K_3Ci - K_2C = 0 \tag{3}$$

4.2.1. Free complexing agent (Cit^{3-}).

(a) At the interface. By assuming that citrate adsorbs on the free area $(1 - \theta)$ and on the covered

area as for a catalytic process, an assumption which will be later justified, the balance for adsorbed citrate is as follows:

$$\beta \frac{d\theta}{dt} = K'C'_0 - K\beta\theta \tag{4}$$

where C'_0 is the free complexing agent interfacial concentration and β the maximal suface concentration of adsorbed $(Cit)^{3-}_{ads}$.

(b) At a distance x from the electrode the citrate concentration C' is given by Fick's second law:

$$\frac{\partial C'}{\partial t} = D \frac{\partial^2 C'}{\partial x^2} \tag{5}$$

where D is the citrate diffusion coefficient, with the boundary conditions for a Nernst diffusion layer of thickness δ:

for $x = \delta$, $C' = 0$. From the comparison between experiment and model it will be shown below that the species issued from the decomplexation probably does not exist in bulk solution. It could thus be (Cit^{3-}) which, in this pH range, is virtually absent

for $x = 0$, $C' = C'_0$ so that

$$K_2 C + D\left(\frac{\partial C'}{\partial x}\right)_0 - K'C'_0 + K\beta\theta = 0 \tag{6}$$

4.2. *Steady-state behaviour*

The values of the reduced copper complex concentration (C) and adsorbed citrate coverage (θ) can be calculated from the steady-state solution of Equations 4 and 5:

$$\theta = \frac{K'K_2 C\delta}{K\beta D} \tag{7}$$

$$C = \frac{i}{2F(K_2 + K_3 i)} \tag{8}$$

At a constant rotation speed, for which the thickness δ of the Nernst layer is constant, the predicted current dependences of C and θ are nearly linear at low current densities and these parameters tend towards a limit of $\frac{1}{2FK_3}$ and $\frac{K_2K'\delta}{K\beta D\, 2FK_3}$, respectively for high current densities. In addition, for a given current density, θ is proportional to δ, i.e. to the reciprocal square root of the electrode rotation speed.

Equation 2 predicts a current dependence of the faradaic efficiency which is almost linear at low current densities with a slope of $\frac{K_3(Cit\ H)}{K_2(Cu)}$. This is in good agreement with the experimental results (Fig. 2). With molecular weights of 190 for $(Cit\ H)$ and 64 for (Cu), the ratio K_3/K_2 would be equal to 2.02 $A^{-1}\,cm^2$.

4.3. *Impedance*

The faradaic impedance can be calculated by linearizing Equation 1

$$\frac{1}{Z_f} = \left(\frac{\partial i}{\partial E}\right)_\theta + \left(\frac{\partial i}{\partial \theta}\right)_E \frac{\Delta\theta}{\Delta E} \tag{9}$$

It follows that:

$$Z_f bi = 1 + \frac{i}{(1-\theta)} \frac{\Delta\theta}{\Delta i} \tag{10}$$

where $\Delta\theta/\Delta i$ can be decomposed as follows:

$$\frac{\Delta\theta}{\Delta i} = \frac{\Delta\theta}{\Delta C_0'} \frac{\Delta C_0'}{\Delta C} \frac{\Delta C}{\Delta i} \tag{11}$$

The terms $\Delta\theta/\Delta C_0'$ and $\Delta C/\Delta i$ are obtained by linearizing Equations 4 and 3, respectively:

$$\frac{\Delta\theta}{\Delta C_0'} = \frac{K'}{K\beta(1 + j\omega\tau)} \quad \text{where } \tau = K^{-1} \tag{12}$$

$$\frac{\Delta C}{\Delta i} = \frac{2FK_2C^2}{i^2} \tag{13}$$

By integrating Equation 5 it follows for $x = 0$ [17] that:

$$\frac{\Delta C_0'}{(\partial \Delta C'/\partial x)_0} = -\frac{\delta \tanh (j\omega\tau_d)^{1/2}}{(j\omega\tau_d)^{1/2}} \tag{14}$$

where $\tau_d = \delta^2/D$ is the diffusion time constant.

The term $\Delta C_0'/\Delta C$ is then obtained by differentiating Equation 6 and combining with 12 and 14:

$$\frac{\Delta C_0'}{\Delta C} = \frac{K_2}{\left[\dfrac{D(j\omega\tau_d)^{1/2}}{\delta \tanh (j\omega\tau_d)^{1/2}}\right] + K'\left(1 - \dfrac{1}{1 + j\omega\tau}\right)} \tag{15}$$

By introducing these terms into Equations 12, 13 and 15 it follows that:

$$Z_f bi = 1 + \frac{2FK_2C\theta}{i(1-\theta)} \left\{ \frac{\dfrac{\tanh (j\omega\tau_d)^{1/2}}{(j\omega\tau_d)^{1/2}}}{(1 + j\omega\tau) + \dfrac{\delta K'}{D} j\omega\tau \left[\dfrac{\tanh (j\omega\tau_d)^{1/2}}{(j\omega\tau_d)^{1/2}}\right]} \right\} \tag{16}$$

The transfer resistance R_t (limit of Z_f when $\omega \to \infty$) and the polarization resistance R_p (limit of Z_f when $\omega \to 0$) are given by:

$$R_t bi = 1 \tag{17}$$

$$R_p bi = 1 + \frac{2FK_2C\theta}{i(1-\theta)} \tag{18}$$

By combining Equations 8, 17 and 18, θ can be calculated:

$$\frac{\theta}{1-\theta} = \left(\frac{R_p}{R_t} - 1\right)\left(1 + \frac{K_3 i}{K_2}\right) \tag{19}$$

It should be noticed that if the adsorption of citrate were not catalytic, the term $(1 - \theta)$ in Equation 19 would have disappeared. The condition $\theta \leqslant 1$ would imply $R_p/R_t < 2$ which does not agree with the experimental results.

By introducing Equations 17 and 18 into Equation 16 the faradaic impedance Z_f can finally be written as:

$$Z_f = R_t + (R_p - R_t) \left\{ \frac{\dfrac{\tanh (j\omega\tau_d)^{1/2}}{(j\omega\tau_d)^{1/2}}}{(1 + j\omega\tau) + \dfrac{\delta K'}{D} j\omega\tau \left[\dfrac{\tanh (j\omega\tau_d)^{1/2}}{(j\omega\tau_d)^{1/2}}\right]} \right\} \tag{20}$$

To simulate an impedance diagram it is necessary to estimate the parameter $K'\delta/D$. By combining equations 7 and 8 it follows that:

$$\frac{K'\delta}{D} = \frac{2F}{i} K\beta\theta\left(1 + \frac{K_3 i}{K_2}\right) \tag{21}$$

The β coefficient can be taken equal to the atom superficial density, $\sim 2 \times 10^{-9}$ mol cm^{-2}. For a low rotation speed of 300 rev min^{-1} for which δ is equivalent to 29 μm in water when $D = 10^{-5}$ cm^2 s^{-1}, it is reasonable to consider a coverage equal to 0.5 for $i = 20$ mA cm^{-2}. Then according to Equation 21 it follows that:

$$\frac{K'\delta}{DK} \simeq 10^{-2}\text{s} \tag{22}$$

For each K value, fixed by the time constant $\tau = K^{-1}$, there is a corresponding value of the parameter $K'\delta/D$. The electrode impedance was calculated from Equation 20 for various values of τ and a diffusion time constant equal to 0.84 s. The double layer capacity, considered in parallel with Z_f was 80×10^{-6} F cm^{-2} and the resistances where $R_t = 4.5\,\Omega$cm^2 and $R_p = 9.7\,\Omega$cm^2, close to the experimental data obtained in 0.6 M sodium citrate electrolyte at 20 mA cm^{-2} with an electrode rotation speed of 360 rev min^{-1}.

With a slow adsorption equilibrium for which τ and τ_d are of the same order of magnitude, the experimental results are not satisfactorily simulated (Fig. 11b). By contrast when the adsorption equilibrium is fast relative to diffusion, i.e. $\tau \ll \tau_d$, the experimental plots are well simulated (Fig. 11a) and this situation can be considered to apply to account for the experimental data. Then the value of θ can be estimated from Equation 19 and from the values of the R_p/R_t ratio measured at various current densities. At a given rotation speed, the current dependence of θ (Fig. 12) is observed to agree with the theoretical predictions of Equations 7 and 8. These equations also predict that θ varies linearly with $\Omega^{-1/2}$ with a slope proportional to C, i.e. to i at low current densities. Fig. 13 shows that this situation is not exactly confirmed: though the linear dependence of θ upon $\Omega^{-1/2}$ is verified the straight lines do not intersect the axes at the origin and their slope is not proportional to the current density. These results thus indicate that Equations 7 and 8 correspond to an oversimplified description of the phenomena.

It must be noted that if the free complexing species issued from the decomplexation exist in bulk electrolyte (at a concentration C'_s) the adsorption would lead to an additional coverage $\theta_0 = K'C'_s/K\beta$ independent of current and hydrodynamic conditions. Then Equations 7 and 21 would become

$$\theta = \theta_0 + \frac{K'K'_2 C\delta}{K\beta D} \tag{23}$$

and

$$\frac{K'\delta}{D} = \frac{2F}{i} K\beta\,(\theta - \theta_0)\left(1 + \frac{K_3 i}{K_2}\right) \tag{24}$$

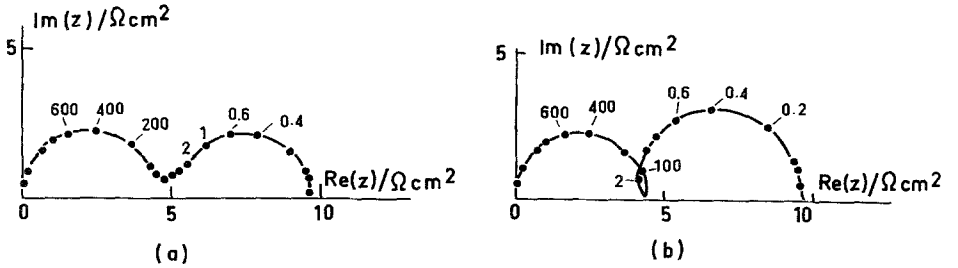

Fig. 11. Complex plane impedance plot simulated by taking $R_t = 4.5\,\Omega$cm^2, $R_p = 9.7\,\Omega$cm^2, $\tau_d = 0.84$ s and $C_{dl} = 80\,\mu$F cm^{-2}. Curve a: $\tau < 1.6 \times 10^{-3}$ s, Curve b: $\tau = 1.6 \times 10^{-1}$ s.

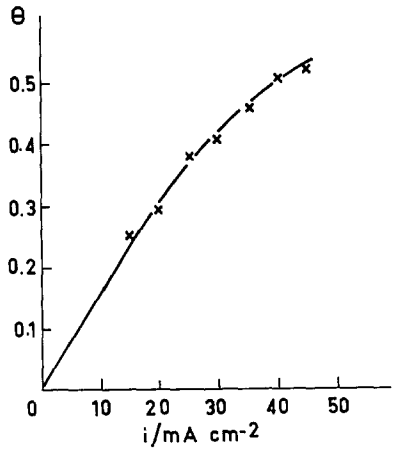

Fig. 12. Electrode coverage by complexing agent as a function of current density in 0.5 M $CuSO_4$, 0.6 M Na_3Cit electrolyte. Rotation speed 1800 rev min^{-1}.

Then for $i = 20\,mA\,cm^{-2}$ a coverage $(\theta - \theta_0)$ equal to 0.5 and satisfying Equation 22 would lead to the unacceptable value of $\theta_0 = 1.7$ for a bulk concentration C_s' of the free complexing species supposed to be 0.1 M. This justifies the idea of a low value of C_s' assimilated to zero in the present model.

As shown in Fig. 4 the $R_t i$ product tends towards a constant value of 100 mV. Thus according to Equation 17 the activation transfer parameter b would be equal to $10\,V^{-1}$. It should be noted that for 0.5 M citrate (Curve 1) the $R_t i$ product increases over a larger current range and does not follow Equation 17 so well. This could be attributed to the fact that the reversibility of the charge transfer Reaction I has been disregarded in the present theoretical approach.

Fig. 7 shows that the frequency f_1 at the apex of the low frequency capacitative feature is nearly proportional to the electrode rotation speed Ω whatever the current is. This is in good agreement with the situation predicted by the model when the diffusion of $(Cit)^{3-}$ is slow as compared to the adsorption equilibrium. In this case:

$$f_1 = \frac{2.5}{2\pi\tau_d} = \frac{2.5D}{2\pi\delta^2} \sim \Omega \tag{25}$$

4.4. *Citrate ammonia electrolytes*

In citrate ammonia electrolytes, where particular dependences of the current efficiency on the

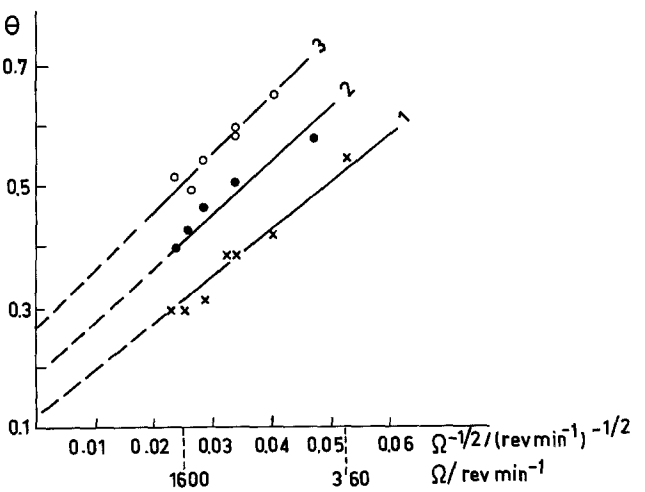

Fig. 13. Electrode coverage by complexing agent as a function of reciprocal square root of the electrode rotation speed in 0.5 M $CuSO_4$, 0.6 M Na_3Cit. Curve 1: $i = 20\,mA\,cm^{-2}$, Curve 2: $i = 30\,mA\,cm^{-2}$, Curve 3: $i = 40\,mA\,cm^{-2}$.

current density and the electrode rotation speed were observed, the electrode behaviour can also be interpreted in the framework of the same model when the discharge of the complexed cupric species C is considered to occur in two consecutive steps (Reactions I and I*) coupled by a monovalent intermediate C* which is soluble and able to diffuse into the bulk electrolyte. The other reactions are the same as for ammonia-free electrolytes:

$$C + e \xrightarrow[(I)]{K_1} C^* + e \xrightarrow[(I^*)]{K_1^*} C^{2-} \qquad (D_1)$$

$$\text{(II)}\quad C^{2-} \xrightarrow{K_2} Cu + Compl^{2-} \qquad \text{(IV)}\quad Compl^{2-} \xrightarrow{D} (Compl)^{2-}_{sol}$$

$$Compl^{2-} \underset{K}{\overset{K'}{\rightleftharpoons}} (Compl)^{2-}_{ads} \qquad \text{(V)}$$

$$\text{(III)}\quad C^{2-} \xrightarrow{K_3} \text{Included species}$$

where $Compl^{2-}$ denotes the free complexing species. The current density results from the two partial current densities i_1 and i_1':

$$i = i_1 + i_1^* = F(1 - \theta)(K_1 \mathscr{C} + K_1^* \mathscr{C}^*) \tag{26}$$

where $K_1 = k_1 \exp(b_1 E)$ and $K_1^* = k_1^* \exp(b_1^* E)$ if both reactions are assumed to have a Tafel behaviour.

The faradaic efficiency would be the product of η_1 and η_2, where η_1 is related to the two parallel paths at the stage of the intermediate C* and η_2 to the subsequent reactions.

$$\eta_1 = \frac{K_1^*}{K_1^* + \dfrac{D_1}{\delta}} = \frac{i_1^*}{i_1} \tag{27}$$

where D_1 is the diffusion coefficient of C*. η_2 is calculated as for ammonia-free electrolytes:

$$\eta_2 = 1 + \frac{K_3 i_1^* (compl)/(Cu)}{K_3 i_1^* + K_2} \tag{28}$$

with

$$i_1^* = \frac{\eta_1}{1 + \eta_1} i \tag{29}$$

the following result is obtained

$$\eta = \eta_1 \eta_2 = \eta_1 \left[1 + \frac{K_3 \eta_1 i (compl)/(Cu)}{K_2(1 + \eta_2) + K_3 \eta_1 i} \right] \tag{30}$$

Equation 27 indicates that η_1 is an increasing function of the potential and thus of the current density, and low values of η_1 at low current densities can explain the Curves 2a and b in Fig. 9.

However, ignoring the value of η_1, the ratio K_3/K_2 cannot be estimated from the current dependence of η as was done in ammonia free electrolytes.

As a consequence the electrode impedance which depends on both η_1 and K_3/K_2, does not allow the electrode coverage θ by the adsorbed complexing species to be evaluated.

From Equations 26 and 27 the transfer resistance R_t is given by:

$$(R_t)^{-1} = i_1 b_1 + i_1^* b_1^* = i_1(b_1 + b_1^* \eta_1) \tag{31}$$

and $R_t i$ product is:

$$R_t i = \frac{1 + \eta_1}{b_1 + \eta_1 b_1^*} \tag{32}$$

Generally this product is not constant as η_1 is an increasing function of the current density unless the two activation coefficients b_1 and b_1^* are equal. Such a situation might exist in ammonia-containing electrolytes at pHs higher than 9.5 where $R_t i$ is observed to be constant and yields $b_1 = b_1^* = 11.8\,V^{-1}$. Moreover the impedance diagrams which exhibit no medium frequency loop, attributable to the relaxation of the surface concentration of C*, corroborates such a situation known to occur when the two activation parameters are equal [4].

5. Conclusion

A reaction path for copper electrocrystallization in citrate electrolytes is developed. It implies the direct discharge of a complexed cupric compound. The reduced complex is either included into the deposit or undergoes decomplexation yielding molecules of free complexing agent which either diffuse towards the solution or adsorb on the electrode surface and partly block it. In the case where the diffusion process of the free complexing agent is slow in comparison with the adsorption–desorption equilibrium, the model explains the main features of the electrode kinetics (impedance plots, polarization curves and current dependence of the current efficiency) observed for sodium citrate concentrations between 0.5 and 0.8 M in the electrolyte.

The electrode behaviour observed in ammonia citrate electrolytes at pHs 9.5 to 10.5 can be accounted for by the same model when considering that the reduction of the cupric complex occurs in two steps coupled by the Cu(I) intermediate able to diffuse into the bulk solution. In the case where both transfer reactions have the same activation parameters with potential the model accounts for the main features of the electrode kinetics (impedance plots and current dependence of the current efficiency).

References

[1] K. Vu Quang, E. Chassaing, B. Le Viet, J. P. Celis, J. R. Roos, *Metal Finishing* **10** (1985) 25.
[2] A. Brenner, 'Electrodeposition of alloys. Principles and Practice', Vol. I, Academic Press (1963) p. 570.
[3] J. R. Roos, J. P. Celis, C. Buelens, D. Gordis in 'Application of Polarisation Measurements in the Control of Metal Deposition' Process Metallurgy Vol. 3 (edited by I. Warren) Elsevier, Amsterdam (1984) p. 177.
[4] E. Chassaing, R. Wiart, *Electrochim. Acta* **29** (1984) 649.
[5] V. Alvarez, S. Gonzalez, A. Arevalo, *ibid.* **29**(9) (1984) 1187.
[6] A. W. M. Verkroost, M. Sluyters-Rehbach, J. H. Sluyters, *Electroanal. Chem.* **39** (1972) 147.
[7] A. Brenner, 'Electrodeposition of Alloys, Principles and Practice', Vol I. Academic Press (1963) p. 399.
[8] J. Lefevre, *J. Chimie Physique* **54** (1957) 597.
[9] R. W. Parry, F. W. Dubois, *J. Amer. Chem. Soc.* **74** (1952) 3749.
[10] K. S. Rajaan, A. E. Martell, *J. Inorg. Nucl. Chem.* **29** (1967) 463.
[11] O. Kardos, *Plating* **61** (1974) 129.
[12] *Idem, ibid.* **61** (1974) 229.
[13] *Idem, ibid.* **61** (1974) 316.
[14] L. Meites, *J. Amer. Chem. Soc.* **72** (1950) 180.
[15] Stability Constants, *The Chemical Society Lond, Special Publication* no 25 (1971).
[16] J. Edwards, *Trans. Inst. Metal Finishing* **41** (1964) 140.
[17] K. S. Cole, 'Membranes, Ions and Impulses', University of California Press, Berkeley (1968) p. 183.